HIGH-RESOLUTION ANALYTICAL ELECTRON MICROSCOPY CHARACTERIZATION OF STRESS CORROSION CRACK TIPS

S. M. Bruemmer and L. E. Thomas

Pacific Northwest National Laboratory
P.O. Box 999, Richland, WA 99352

ABSTRACT

Recent results are presented demonstrating the application of cross-sectional analytical transmission electron microscopy (ATEM) to corrosion and cracking in high-temperature water environments. Microstructural, chemical and crystallographic characterizations of buried interfaces at near-atomic resolutions are shown to reveal evidence for unexpected local environments, corrosion reactions and material transformations. Information obtained by high-resolution imaging and analysis indicates the corrosion and deformation processes during crack advance and provides insights into the mechanisms controlling environmental degradation. Examples of intergranular attack and cracking in type 316 austenitic stainless steel and Ni-base alloy 600 are presented to illustrate the value of this approach. The presence of deeply attacked grain boundaries off the main cracks, revealed by TEM, is believed to indicate a major role of active corrosion in the stress-corrosion cracking (SCC) process. Corroded boundaries were filled with oxides to the leading edges of attack. Analyses of the oxide films and impurities in intergranular penetrations and crack tips with widths of 10 nm or less indicate influences of the grain boundary characteristics and the water chemistry. Boundary and precipitate corrosion structures can be used to identify the local electrochemistry promoting degradation in complex service environments. Solution impurities such as Pb are found in high concentrations at nm-width reaction zones in samples from steam-generator secondary-water environments indicating water access at leading edges of the attack and the influence of these impurities on the corrosion processes. Results for specific samples are used to demonstrate the ability of cross-sectional ATEM to reveal new details of buried corrosion structures that cannot be detected by other methods.

KEYWORDS

Crack tips, stress corrosion cracking, corrosion, intergranular fracture, grain boundary, segregation, corrosion products, passive films, solution impurities, deformation.

INTRODUCTION

The fundamental basis for mechanistic understanding and modeling of stress corrosion cracking (SCC) remains in question for many systems. Specific mechanisms controlling SCC can vary with changes in alloy characteristics, applied/residual stress or environmental conditions. The local crack electrochemistry, crack-tip mechanics and material metallurgy are the main factors controlling crack growth. These localized properties are difficult or impossible to measure in active cracks. Nevertheless, it is essential to quantitatively interrogate these crack-tip conditions if mechanistic understanding is to be obtained.

A major recent advance has been the ability to investigate SCC cracks and crack tips using analytical transmission electron microscopy (ATEM). ATEM enables the characterization of SCC cracks including trapped solution chemistries, corrosion product compositions and structures, composition gradients and defect microstructures along the crack walls and at the crack tip. A wide variety of methods for imaging and analyses at resolutions down to the atomic level can be used to examine the crack and corrosion film characteristics. Surface films and reaction layers have been examined by cross-sectional TEM techniques, but limited work had been conducted on environmentally induced cracks until recently [1-7]. A critical aspect of the recent work has been the development of sample preparation methods in which the crack corrosion products are protected during the ion-thinning process by embedding the cracks with a low-viscosity thermoplastic resin. This capability combined with modern ATEM techniques has enabled new insights into corrosion processes occurring at buried (limited communication with the bulk environment and surface electrochemical conditions) interfaces and is being used to identify mechanisms controlling SCC in service components.

The objective of this paper is to demonstrate capabilities of cross-sectional ATEM for the characterization of buried crack tips and corrosion interfaces at high resolution. New results are highlighted focusing on SCC in Fe- base and Ni-base stainless alloys. Examples are chosen to illustrate nanometer-scale structures that can only be examined effectively by ATEM methods.

CRACK-TIP SAMPLE PREPARATION AND CHARACTERIZATION APPROACH

The preparation of cross-section samples with suitable electron-transparent areas for high-resolution ATEM characterization was critical for the present work. The first step involves protecting the cracks by vacuum-impregnation with a low-viscosity thermosetting resin. Following impregnation, the section containing cracks is cut out and embedded in a stainless steel tube. The composite sample is then sliced with the main crack in cross section near the disk centers and mechanically polished. Dimple grinding is used to create a bowl-shaped depression at the area of interest. Thinning is then continued from both sides by low-angle ion micromilling with final milling performed at reduced beam energy and incident angle to remove most visible ion damage. Repeated cycles of ion thinning and TEM examination are applied to obtain suitably thin areas at crack tips or other locations of interest. Crack tips represent one of the most difficult regions to effectively protect, prepare and characterize. In nearly all the high-temperature water cases examined so far, cracks are heavily branched and are filled with corrosion products. It is possible that some of these products form during cooling from service temperatures, but most of the oxide phases are expected to form in high-temperature water and will probably restrict crack closure. A detailed description of cross-section sample preparation and possible artifacts has been published elsewhere [3,4].

ATEM characterizations were performed using a 200 kV field-emission-gun TEM with a thin-window, energy-dispersive x-ray spectrometer (EDS) and a parallel-detection electron-energy-loss spectrometer (PEELS) for microchemical analysis. High-resolution ATEM methods were used to analyze the narrow corrosion features near crack tips and along attacked grain boundaries. Besides conventional brightfield and precipitate darkfield imaging, these methods included crystal lattice imaging with Fourier-transform diffraction analysis, fine-probe (0.7-nm diameter) compositional analysis by EDS and PEELS, and fine-probe parallel-beam diffraction with electron probes as small as 5 nm in diameter. In addition, stereoscopic TEM photographs were used to observe finely porous structures along attacked grain boundaries. A Fresnel (off-focus) image contrast method was employed to reveal fine pores and other structures as small as 1 nm.

EXAMPLES OF CRACK-TIP CHARACTERIZATIONS

Results from 316SS and alloy 600 materials that experienced intergranular (IG) SCC in high-temperature (250-320°C), deoxygenated water environments are used to illustrate high-resolution characterizations of crack-tip, crack-wall and corrosion structures. Specific information on water environments and material conditions is given elsewhere [4-7].

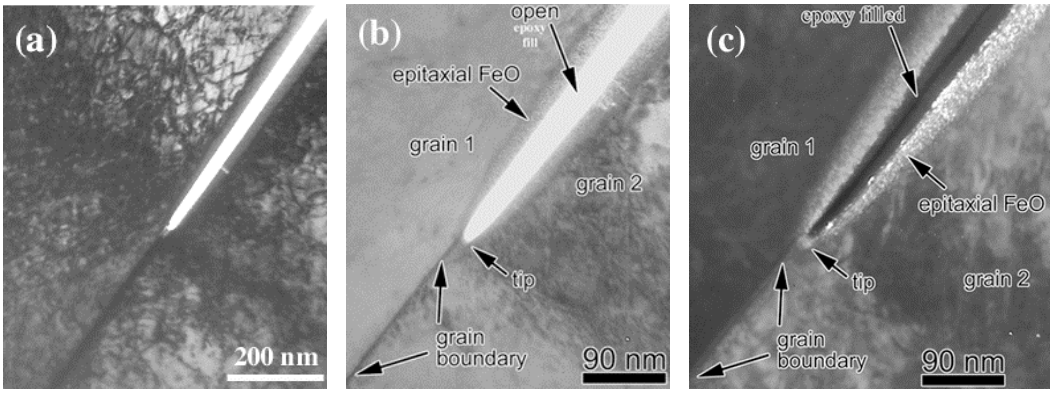

Figure 1: Example of a typical crack tip in the 316SS samples: (a) bright-field image with matrix dislocation structure in contrast, (b) bright-field image with matrix structure out of contrast to elucidate crack tip, and (c) FeO darkfield image highlighting epitaxial oxide on wall and at tip.

Crack-Tip Characterization in 316SS

The 316SS samples that will be discussed were removed from a service component after many years in a 250-290°C, deoxygenated water environment [6,7]. Cracked samples from several locations have been examined and many crack tips characterized. In nearly all cases, wide (>~0.5 μm) cracks were filled with a multi-layer corrosion product oxide, consisting of a Cr-rich FeO and spinel inner layer plus large-grained magnetite (Fe_3O_4) filling the center of the crack. This multi-layer film is similar to that reported at stainless steel surfaces [8,9] with the exception of the FeO-structure oxide. The focus here is on the crack tips as illustrated in Figure 1. A somewhat "classic" appearance of a SCC crack tip in a passive alloy is seen with a non-porous, epitaxial FeO-structure oxide film on the walls. The crack narrows to ~10 nm at the tip comparable to the oxide film thickness ahead of the tip and on the adjacent crack walls. Evidence of significant deformation (high dislocation density) is present in the metal surrounding the tip as illustrated in Figure 1(a), but localized slip bands have not been observed intersecting the crack. However, twins are seen at or near primary or secondary crack tips as demonstrated in Figure 2. Scanning electron microscopy indicates that most twins are present before the propagation of SCC cracks and that many cracks end at intersections of twins with grain boundaries [10]. The examples presented in Figure 2 show deformation twins immediately ahead of a crack tip in (a) and a crack that has propagated through several twins in (b). Oxide films at these crack tips were again found to be non-porous, but were predominately a nanocrystalline FeCr spinel versus the epitaxial FeO-structure oxide seen at other tips. Low levels of solution impurities (e.g., Na) were discovered in the oxides indicating that a caustic environment may have been in cracks.

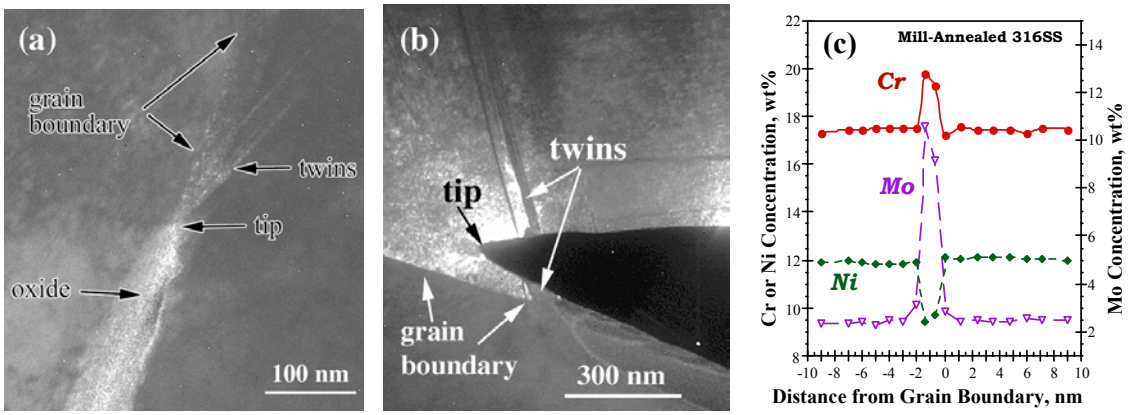

Figure 2: Crack-tip interactions with matrix twins in a 316SS sample with twin present immediately ahead of the crack tip in (a) and immediately behind the tip in (b) where the crack is clearly displaced off the grain boundary plane. The composition profile in (c) was taken across the grain boundary in a non-attacked base metal region well ahead of the crack tip.

A final important crack characteristic illustrated in Figures 1 and 2(b) is the crack-tip locations that are often adjacent to, and not centered on, the grain boundary. Crack propagation along a path several nm off the boundary was clearly evident at about one-third of the crack tips examined. The only measured material feature in these mill-annealed 316SS samples that may play a role is the grain boundary composition. Significant Mo and Cr enrichment is present at grain boundaries as shown in Figure 2(c). This non-equilibrium segregation has been seen in many mill-annealed stainless steel heats (often with B enrichment) and is most likely produced during initial processing before service [11]. The profile presented was obtained ahead of a crack tip that was centered off the boundary interface and it reveals the maximum segregation adjacent to the boundary. It is possible that the altered local composition influences dissolution and passivation, thereby SCC propagation.

Intergranular Attack and SCC in Alloy 600

Recent work [3-7] on cracked alloy 600, pressurized-water-reactor (PWR), steam-generator tubes has shown a remarkable tendency for IG attack along with SCC. TEM examinations of samples cracked in various high-temperature water environments has revealed narrow oxidized zones, 5-to 20-nm in width and up to tens of μm in length, along nearly every intersected grain boundary in the wakes of cracks. An example of these IG corrosion zones is shown in Figure 3 for mill-annealed alloy 600 after long-term exposure to PWR primary water at 330°C. TEM images show no visible cracks in the corrosion zones and no significant deformation of the surrounding metal matrix. Fresnel contrast imaging in Figure 3(a) shows that these structures are highly porous on a scale of 1-2 nm. Electron diffraction analyses revealed that the corrosion product consisted of nanocrystalline oxides (NiO, Cr_2O_3 and/or spinel depending on the particular environment). Lattice imaging identified individual crystallites with sizes down to a few nm as demonstrated in Figure 3(b). The fine porosity at the tip of a corrosion zone is illustrated in Figure 3(c). A complex network of nm-size voids and tunnels is present in the narrow oxide layer along an inclined grain boundary, as well as voids along the grain boundary plane ahead of the tip. The oxide at the attack tips was Cr_2O_3, even though the predominant oxide some distance (>100 nm) behind the tip was NiO (Cr and Fe levels similar to the matrix). Significant Cr enrichment at the oxidized tip was measured by high-resolution EELS, but the adjacent matrix was not depleted. The observation of pores in the metal ahead of the oxidation front suggests that vacancies may be injected during the corrosion process. Due to the narrow dimensions of the corroded IG zones in alloy 600, these structures have been undetectable by other examination methods including optical metallography, SEM or secondary-ion mass spectroscopy.

Exposure to secondary water or steam environments can produce similar IG attack and aggressive degradation of precipitates in alloy 600 samples [6,7]. An example of this behavior is shown in Figure 4 for once-through steam generator tubing removed from the high-superheat (steam) region. Alloy 600 tubing is put into service in the stress-relieved and sensitized condition with closely spaced

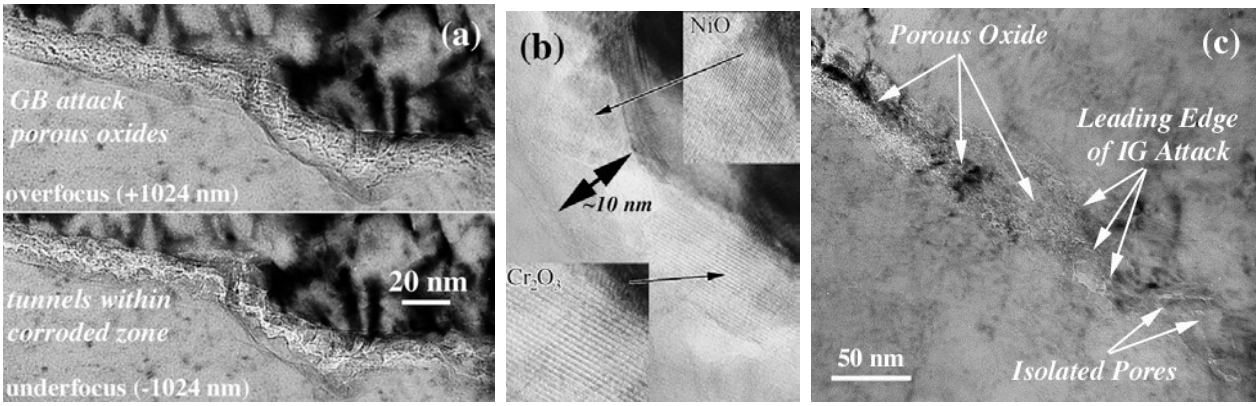

Figure 3: Intergranular attack of alloy 600 in high-temperature PWR primary water: (a) Fresnel contrast images showing narrow porous oxidized zone, (b) lattice images identifying crystallites of Cr_2O_3 and NiO in the corroded zone and (c) leading edge of attack with oxidized material ending within grain boundary plane and presence of isolated pores ahead of corroded region.

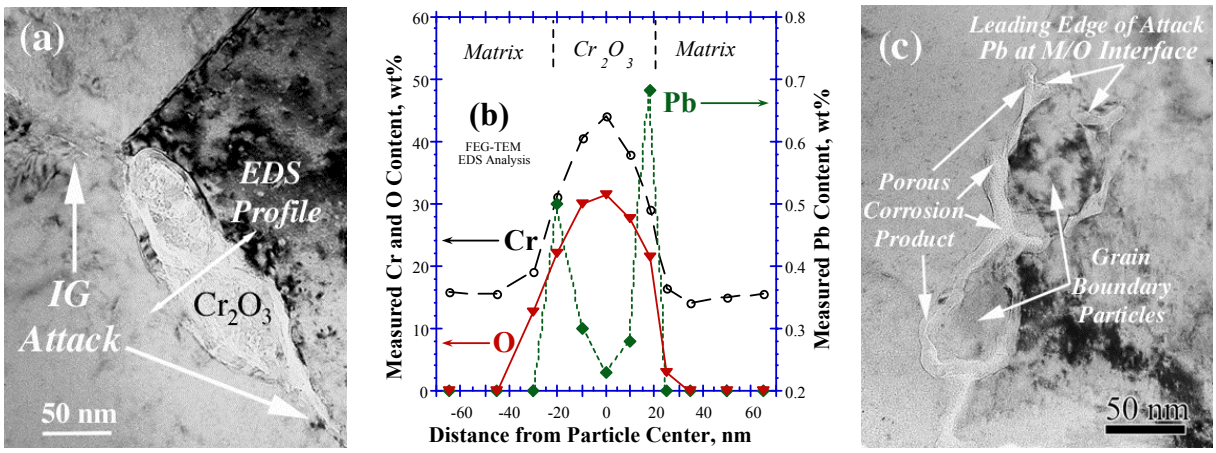

Figure 4: Intergranular attack of alloy 600 in high-temperature PWR secondary water: (a) former grain boundary Cr carbide converted to Cr oxide, (b) composition profile across attacked particle showing Pb enrichment at the metal-oxide (M/O) interface and (c) porous corrosion product oxides around grain boundary particles with Pb present at leading edge of attack.

Cr_7C_3 carbides and $Ni_{23}B_6$ borides. The porous oxide structure in the IG attack zones was similar to the primary-water samples, but the carbides were converted to fine-grained Cr_2O_3 oxides and borides were completely removed. Solution impurities appear to have a strong influence on the stability of these particles. EDS analyses of the oxidized particles (Figure 4a) revealed that environmental impurities, notably Pb, had penetrated the structures and concentrated in the reaction layers along the metal-oxide interfaces (Figure 4b). Further observations at the leading edges of attack showed tunnel-like corrosion zones formed around the IG particles as presented in Figure 4(c). A penetrative porous oxide is seen to envelop a partially converted Cr_7C_3 precipitate and end adjacent to a Ni-rich particle (former boride). The corrosion product in these tunnels consisted of nanocrystalline Cr-Ni spinel containing high concentrations of Pb at the leading edge of attack. This is consistent with Pb promoting dissolution and/or impairing passivity to enhance boundary and precipitate degradation.

DISCUSSION

The application of high-resolution ATEM methods to buried corrosion interfaces in stress-corrosion cracked materials has revealed important details of the degradation processes and mechanisms. This advance comes from two developments: (1) improvements in cross-sectional sample preparation on cracked materials, and (2) the availability of FEG TEMs that allow structural, compositional and crystallographic analyses at resolutions down to atomic dimensions. Significant findings of this continuing research include the recognition that active-path corrosion of grain boundaries plays a major role in SCC of alloy 600 in a wide variety of steam generator environments. This IG attack produces a remarkably thin (<20 nm in width) band of porous, non-protective oxide that extends for many μm. It is clear that water (or steam) penetrates throughout corroded structures. No evidence of plastic deformation was found associated with the IG attack and it appears that plasticity is not required for grain boundary degradation to occur. However, it is likely to accelerate growth rates via a stress-assisted corrosion process. Solution impurities such as Pb are shown to concentrate along the narrow (few nm) reaction layers at buried interfaces. High impurity enrichments at the leading edge of attack suggest that Pb promotes metal (and precipitate) dissolution and/or impairs oxide formation.

Secondary cracking was found in the austenitic stainless steel samples, but no evidence of significant IG attack. The formation of non-porous, protective oxides on crack walls and at the crack tip is more consistent with a classical SCC slip-oxidation mechanism. Crack-wall films are in general agreement with surface films reported on stainless steels after high-temperature water exposure. The presence of the FeO-structure inner film was unexpected and it appears to have a close structural relationship with the spinel phase that forms adjacent to this oxide. In general, non-porous protective films tend to form on exposed 316SS surfaces in these high-temperature water environments, while porous, non-

protective oxides are produced in the alloy 600 cracks and attacked boundaries. Cracks are generally quite tight (tip openings down to a few nm) in both alloys, but the 316SS samples reveal a high dislocation density at all crack tips suggesting that plasticity is an essential part of the SCC process.

This work has demonstrated the ability of ATEM to reveal new and important details of buried corrosion and SCC structures that cannot be detected by other methods. However, the current observations must be considered work in progress and additional work is needed to properly establish mechanisms controlling IGSCC. In particular, ATEM characterization of degradation structures must be performed on samples where mechanisms are better distinguished. Tests in high-temperature aqueous and gaseous environments should be performed under well-controlled solution chemistries and electrochemical conditions to establish a library of the corrosion signatures.

CONCLUSIONS

Cross-sectional ATEM has been used to effectively characterize corrosion and cracking in high-temperature water or steam environments. A wide variety of high-resolution imaging and analysis methods are employed to elucidate processes occurring during crack advance and provides insights into the mechanisms controlling environmental degradation. Fundamental differences are detected between corrosion structures in Fe-base and Ni-base stainless alloys. Deeply attacked grain boundaries off the main cracks are found in alloy 600 samples indicating a major role of IG corrosion in the SCC process. Corroded boundaries were filled with nanocrystalline oxides to the leading edges of attack. Precipitates in alloy 600 are also attacked and can be used to identify the local electrochemistry promoting degradation in complex service environments. Solution impurities such as Pb are found in high concentrations at nm-width reaction zones in samples from secondary-water environments documenting water access at leading edges of the attack and indicating how impurities influence the corrosion processes. Results presented demonstrate the ability of cross-sectional ATEM to reveal new details of buried corrosion structures that cannot be detected by other methods.

ACKNOWLEDGEMENTS

The technical assistance of C. E. Chamberlin and V. Y. Gertsman are recognized along with helpful discussions with P. M. Scott. Primary support comes from the Materials Sciences Branch, Office of Basic Energy Sciences, U.S. Department of Energy (DOE) under contract DE-AC06-76RLO 1830 with Battelle Memorial Institute. Additional support is acknowledged from EPRI, the B&W Owners Group Chemistry Committee and the DOE Office of Nuclear Energy, Science and Technology.

REFERENCES

1. Lewis, N., Perry, D.J. and Bunch, M.L. (1995) In: *Proc. Microscopy and Microanalysis* ed., Bailey, G.W. et al., Jones and Begnell Publishing, New York, 550.
2. Lewis, N., Attanasio, S., Morton, D.S. and Young, G.A. (2001) In: *Proc. Staehle Symposium on Chemistry and Electrochemistry of Corrosion and Stress Corrosion*, ed. Jones, R.H. TMS, p. 421.
3. Thomas, L.E., Charlot, L.A. and Bruemmer, S.M. (1996) In: *Proc. New Techniques for Characterizing Corrosion and Stress Corrosion*, Eds. Jones, R.H. and Baer, D.R. TMS, p. 175.
4. Thomas, L.E. and Bruemmer, S.M. (2000) *Corrosion J.*, 56, 572.
5. Thomas, L.E. and Bruemmer, S.M. (2000) In: *Proc. 9th Int. Conf. Environmental Degradation of Materials in Nuclear Power Systems-Water Reactors*, ed. Bruemmer, S., Ford, F.P., TMS, p. 41.
6. Bruemmer, S.M. and Thomas, L.E. (2001) In: *Proc. Staehle Symposium on Chemistry and Electrochemistry of Corrosion and Stress Corrosion*, ed. Jones, R.H. TMS, p. 123.
7. Bruemmer, S.M. and Thomas, L.E. (2001) *J. Surface and Interface Analysis*, in press.
8. Robertson, J. (1991) *Corrosion Sci.*, 32-4, 443.
9. Stellwag, B. (1998) *Corrosion Sci.*, 40-2/3 337.
10. Gertsman, V.Y. and Bruemmer, S.M. (2001) *Acta Metallurgica*, 49, 1589.
11. Karlsson, L. (1988) *Acta Metalurgica*, 36, 1.